

The b1 Collaboration Response to TAC and iTAC Comments

The b1 Collaboration

June 7, 2013

1 TAC Technical Comments

As mentioned by the TAC typical drifts in Hall C in the factors used to normalize the scattering rate can create relatively large false asymmetries of $\pm O(0.01)$, we can show that these effects are manageable as the experiment is proposed. We also look forward to taking advantage of the upgrades to the Hall C infrastructure. Our collaboration is unique for this experiment in that the group contains a large fraction of Solid Polarized Target physics researchers. This gives the advantage of novel approaches as well as the expertise needed for the installation and operation of the polarized target.

1.1 Drift Mitigation

1.1.1 Charge

The uncertainty estimate in charge that results in a small absolute change in the observable is described in the proposal in the section entitled ‘Time Dependent Factors.’ We also include a separate error from charge in the table of systematics. Analytically there is a component of uncertainty that propagate with the other relative errors and only a very small piece that results in a drift in the observable. The resulting expression for the charge and other contributions to the drift in the observable is expressed as,

$$\delta A_{zz}^d = \pm \frac{2}{fP_{zz}} \delta\xi, \quad (1)$$

where $\delta\xi$ contains the sum of δQ , $\delta\epsilon$, δl , and δA . This means that to accurately represent δA_{zz}^d we must obtain only the residual deviation from the two polarization states in the time span of a single cycle (sampling of that data point). The value used for δQ is an estimate based on the actual effect seen in an observable which helps us to separate the relative contribution from the drift in a given time frame. The beam charge asymmetries using the luminosity monitors for experiment E06-010 resulted in a absolute drift in the asymmetry of 2.2×10^{-4} . An additional estimate on the change in the BCM calibration constant is seen in experiment E08-027 resulting in a absolute deviation of 2.0×10^{-4} over the course of six days. We expect to be able to minimize

long term drifts by careful thermal isolation of the BCMs, however resulting trends will be studied and corrections implemented. We do consider it a priority to monitor and correct for remaining temperature dependence. In addition we look forward to further reduction through the use of the new low power Faraday Cup. We estimate a drift in the observable to be no larger than 3×10^{-4} including the effects from the change in current for our configuration from the estimates used.

1.1.2 Trigger-Tracking

For the most part an easy way to determine whether or not the error will lead to an effect on drift is to determine if the change over time is seen in one polarization state and not the other with respect to the observable. Effects from trigger, cuts and tracking efficiency do lead to errors in normalization, however both polarization states see the same stochastic fluctuation over the course of a cycle leading only to a small relative uncertainty in the observable. Aspects of the error that are non-stochastic and follow an unknown trend have been estimated in the proposal under the name ‘detector drifts.’ Recently we obtained a secondary estimate based on HRS detector stability using Hall A transversity data for detected pions. The resulting drift was 2.2×10^{-4} . In addition we intend to set detector thresholds conservatively and use meticulous on-line monitoring and checks to the relative changes in tracking efficiency between slugs. For our present estimate including trigger, tracking, cuts, and detector errors that show up strictly as an absolute drift in the observable we estimate no larger than 3×10^{-4} .

1.1.3 Target Dilution and Length

There are presently UVA designs for target cup and material fabrication to minimize the probability of changes to target dilution in the form of material loss over time. The cup contains multiple hole arrays that are only a 0.1 mm in size. The material shape and consistency is optimized to maximize the packing fraction and minimize the fracturing capacity. The ammonia is hand selected to reduce the structural faults to obtain beads approximately 2 mm in diameter which have already undergone multiple steps of mechanical stress including being pre-irradiated at NIST with a 10 μ A beam. The temperature and thus the density of the target is kept the same in both polarized and unpolarized states. There are four temperature sensors in a standard solid polarized target setup that can be used to monitor this. The temperature is controlled via LHe evaporation, microwave, and beam heating. All three are used to maintain consistent temperature in both polarization states. With these precautions we consider some estimates of the possible drift involved.

The averaging of the target length done by the rasters results in an effective length that is determined by the fraction of the cup volume (equivalently, the rastered volume) that is filled with ammonia [1]. A possible change in the effective target length between the polarized and unpolarized periods of a measurement cycle could come from a net change of material in the raster volume. Since the raster diameter is 25% smaller than the cup diameter, there is always material outside the raster

region that would fill in an unlikely loss in the rastered region. A possible estimate of the length change can be obtained by considering the ratio of the 0.008 cm^3 volume of a fragment to the 6.8 cm^3 raster volume (including packing fraction) the ratio is $\sim 1/850$.

The only documented instance with ammonia polarized targets and CEBAF $\sim 100 \text{ nA}$ beams of a possible rearrangement of material about the target NMR coil that might indicate an associated net change in material was seen during E07-003, SANE, which took about 500 hours of $\geq 85 \text{ nA}$ beam. During one 20 h polarized and unpolarized cycle, the loss of 1 or 2 fragments would result in a $\sim 1 \times 10^{-3}$ change in target length, with a $\sim 20\text{h}/500\text{h}$ probability or, potentially, a 1×10^{-4} difference in target length between the cycle halves. No instances of material fragmentation, which could potentially lead to net losses in the raster region have been observed with up to 150 nA CW CEBAF beams (E93-026, E01-006, E07-003).

The only instances of material fragmentation for ammonia targets were observed at SLAC, in the E143/E155/E155x series of experiments, but the SLAC beam is pulsed, with $4 \mu\text{s}$ wide pulses of $\sim 20 \mu\text{A}$ current at 120 Hz repetition rate. Such beam time structure can be expected to damage the ammonia crystals by thermal shock. In fact, to further prevent possible shock effects at JLab, the polarized target experiments in Hall C implemented the procedure of gradual ramping up of the beam current after beam trips.

All changes to the material that occur during movement of the target ladder or annealing can only happen at the end of each pair of measurement cycles and are irrelevant for the preceding or following cycles. Small changes to material NMR loop coupling are consistent to both polarization states and exist as a relative error in the polarization. In addition as long as the LHe is superfluid ($< 2 \text{ K}$), its flow can not lead to material rearrangements. The LHe that is feed at the bottom of the nose piece coming from the separator is below 2 K so emptying and refilling does not have any effect.

Depolarization using LHe is a relatively standard technique. In this procedure the beam is turned off and the LHe fill valve that controls the LHe level that surrounds the target insert is slowly reduced as to not replenish the LHe evaporation until the material has warmed up and the polarization has died out. The LHe is gradually filled again as in the standard evaporation mode and again set on automated control. Once the material is unpolarized and again submerged under the LHe the microwaves are turned on in off resonance mode. The unpolarized target is then ready for beam. This procedure provide a quick way to kill polarization while returning the unpolarized state to the exact condition of the polarized state. The small fluctuation in density, temperature and NMR material couple occur in both states and are a small relative error in the polarization. All other aspects that may result in addition to the drift are negligible.

For example the target operating temperature is $\sim 1.1 \pm 0.15 \text{ K}$, well below the superfluid point. Over that range, the LHe density, changes by 4×10^{-5} (the density actually increases below $\simeq 1.1\text{K}$ and increases above, by about equal amounts over the temperature interval [2]). The lattice constant of deuteroammonia [3] changes from 5.048 \AA at 2 K to 5.073 \AA at 77 K , corresponding to a 1×10^{-5} change over

the ± 0.15 K interval considered above. For a 60% packing fraction the change would be 2.3×10^{-5} for a 0.15 K unexpected temperature difference between polarization states. Any possible unaccounted changes in target length between the polarized and unpolarized parts of each cycle can also be monitored by recording the time dependence of the luminosity with a $\simeq 0.5 \times 10^{-4}$ accuracy. It's our understanding that such device is available in the Hall.

In summary, we consider that the contribution of the non-statistical time dependence of the target length to the measurement error will not exceed one part in 10,000 for each cycle. In the possible occurrence of target bead shifts the effect is easily averaged out in the rastered volume to be negligible as is the loss of a bead during a single polarization cycle.

1.1.4 Solid Angle

The error that arises in the observable due to beam position and magnet currents over time is inherently very difficult to separate into drift and relative uncertainty. The 0.1% error over a 12 hour period is probably quite accurate however being that both polarization states experience the same fluctuations we believe that the majority of the uncertainty is relative. There are also concerns on acceptance due to beam position drift. Beam drift can be monitored during the experiment and accounted for during analysis. We consider the largest part of this uncertainty to also be a relative contribution to both target states. The contribution to the drift can be minimized with the feedback system built for parity experiments (regression).

We also agree that the effects that contribute to the drift are critical to pay attention to. Trends that arise from dependence of yield on magnet currents in detectors are a concern related to the spectrometer acceptance. The drift effect can be made to be small, for HRS typically less than 10^{-4} for the dipole and 10^{-3} for the three quads. We assume similarly for HMS. The affects on the acceptance can be determined and corrected through careful analysis. Naturally the target magnet current does not need to be changed between cycles, the uniformity, stability, and setability pointed out in the proposal eliminate field variation between the two polarization states. We expect a residual drift from solid angle effects after such correction to be no larger than 0.01%. This value was already accounted for in Section 1.1.2.

2 Final Drift Estimate Per Point

Using the values present here for each component that can contribute to the drift we obtain a value no larger than 6×10^{-4} in A_{zz} . We see this as an over estimate of what we can achieved using the out-lined mitigation techniques. To then determine the actual error over the course of the experiment we look at the number of measurements at each point (number of cycles at each point). Since the times at each point are different, the number of cycles is not the same for all points. There are only three independent points, since the HMS data is collected in parallel. For the $x = 0.15$ we intend to double the number of cycles in order to minimize the drift for that point.

x	Hours	Stat. Error	Cycles	Drift Error (10^{-3})
0.15	144	0.15	12	3.2
0.30	216	0.39	9	3.7
0.45	360	0.50	15	2.9
0.55	720	0.37	36	1.9

Table 1: The estimated drift of the A_{zz} asymmetry measurement.

For the other points the need for statistics outweighs the need to reduce the drift. Table 1 shows the resulting drift in the asymmetry for each independent kinematic point in x .

3 Improving Polarization and Errors

The UVA target group has been able to acquire 50% vector polarization with the trend in polarization still increasing. This is with the standard UVA pump system at the university. The UVA pump system now at Jefferson Lab has much greater cooling power. We expect to be able to achieve a tensor polarization much greater than the 12% mentioned by the TAC, even without hole-burning. In addition developments are underway that can be used to measure the polarization after hole-burning. The lack of measuring capacity and large polarization uncertainty has been the biggest block for employing the hole-burning technique. The development and implementation of the technique has broad implication for experiments to come.

3.1 Line Shape Fitting

The SMC group have developed an analytic model [4] of the deuteron absorption function used to determine the deuteron vector polarization. The absorption function model includes dipolar broadening and a frequency-dependent treatment of the intensity factors. The TE signal data can be used to adjust the model for Q-meter distortions and dispersion effects. Once the Q-meter adjustment is made, the enhanced polarizations determined by the SMC fitting and TE-calibration methods compare very well within the accuracy of each method.

The spin system can be irradiated by radio frequency (RF) energy and if that irradiation occurs at the Larmor frequency the spins either absorb or emit some energy. The response of a spin system to RF irradiation is described by its magnetic susceptibility which leads to a direct relation of the ensemble spin system population of states and the area of the signal voltage as a function of the real part of the magnetic susceptibility and RF frequency ω . The polarization for the deuteron can be expressed as,

$$P = C \int \frac{\omega_d S(\omega)}{\omega} d\omega. \quad (2)$$

Where C is a constant the frequency-independent gains in the Q-meter, the $S(\omega)$ is

the NMR signal for the deuteron absorption function whose maximum occurs at its Larmor frequency ω_d only extends over about a $2\pi \times 300$ kHz range, outside of which the dispersion function can be considered to have constant value. This relationship means that the total integrated area of the NMR signal is directly proportional to the material polarization that is inductively coupled to the NMR coil. The polarization from the integrated area is sensitive to spin-temperature and lattice decay.

The SMC model uses first-order quadrupole splitting with electric field gradients. The symmetry configuration of the deuteron and corresponding bonds leads to local electric field gradients that couple to the quadrupole moments of the deuteron causing an asymmetric splitting of the energy levels into two overlapping absorption lines. The two peaks seen in the shape of absorption lines reflect the net number of spins available for making a particular transition.

For a given value of the angle between the axis given by the deuteron bond and the magnetic field there are two resonant frequencies in this system which correspond to the positive $E_0 \leftrightarrow E_1$ transition with energy $\Delta E_+ = E_0 - E_1$ and intensity I_+ and the negative $E_{-1} \leftrightarrow E_0$ transition with energy $\Delta E_- = E_{-1} - E_0$ and intensity I_- .

A fit function based on this model which uses the dipolar broadening of the density of states with a Lorentzian convolution was also developed by the SMC group. The result is a fit function to obtain the intensities I_{\pm} of the two overlapping absorption peaks. The relation $r = I_+/I_- = n_+/n_-$ assume a Boltzmann distribution among the sub-levels so that the vector polarization can be expressed as

$$P = (r^2 - 1)/(r^2 + r + 1), \quad (3)$$

and the tensor polarization can be expressed as,

$$P_{zz} = (r^2 - 2r + 1)/(r^2 + r + 1). \quad (4)$$

For vector polarization above 30% the line shape fitting technique can be made accurate to 3%. The great advantage here is that the error in area and calibration constant from the TE-calibration are completely side stepped. The majority of error from the fitting technique is fitting error and background subtraction. This is especially useful for determining the tensor polarization as compared to using the analytic relation $P_{zz} = 2 - \sqrt{4 - 3P^2}$ for which the polarization error propagates to roughly double. Using the line shape fitting combined with a cold NMR [6] it is within reason to expect to be able to cut our polarization uncertainty listed in the proposal by 50%. The cold NMR reduces systematic effects over time significantly. This type of improvement is a simple extension to the standard Q-meter NMR system and has been used by UVA and the Jlab target group. The UVA target group has the cold NMR available for experiments. In addition the UVA target group is presently devolving a fitting algorithm based on the SMC peak asymmetry fitting technique.

3.2 Optimizing Polarization Through RF-saturation

The technique of manipulating the fraction of the spins in the magnetic sub-levels with a saturating RF field can be done in such a way as to optimize the resulting tensor

polarization. The optimization is done by irradiating the sample with a frequency-modulated RF field around the peak and pedestal position for either the $E_{-1} \Leftrightarrow E_0$ or $E_0 \Leftrightarrow E_1$ transitions. RF saturation takes about 10 minutes leaving the $m=0$ and the $m=\pm 1$ with approximately the same populations. The population of the $m=0$ level will have been increased relative to the Boltzmann population level leading the tensor polarization to increase to the same degree. For complete saturation the initial vector polarization and resulting tensor polarization are equal in magnitude neglecting any relaxation during the procedure, this would imply tensor polarization of 40-45% is very plausible. Even without complete saturation it has been shown that the tensor polarization can be roughly doubled as compared to what is achievable with microwaves alone [5]. These results need verification and further study but are very promising to our objective. Improvement to the expected polarization, although not strictly necessary, would allow the addition of kinematic points, improved statistical accuracy and the reduction of the error contribution from drift δA_{zz}^d . The reduction to this error is seen analytically in Eq. 1. The value of δA_{zz}^d is reduce by the same factor that the polarization is increased.

3.3 Measuring the RF-saturation Signal

It is important to measure the dynamic NMR signal for all possible line shapes and spin state populations through the experiment. This can be done by using an extension to the line shape fitting technique which relates the area of the fitted absorption lines to the population of states. Through the course of the hole burning RF modulation the dipolar broadening of the density of states is altered in a calculable way. For example an area translation from the $m=0 \rightarrow m=1$ transition to enhance tensor polarization can be measured by comparing the fitted area from the SMC method prior to hole burning RF modulation with a Riemann sum of the reduced region. The ratio, r_0 , of the remaining non-translated area to the initial area gives the fractional increase from the available enhancement to the tensor polarization. The increase to the tensor polarization relative to the Boltzmann population level can then be added to the previously measured initial tensor polarization (prior to RF modulation). The hole burning tensor polarization can be expressed as,

$$P_{zz}^{HB} \approx \frac{A^{NMR}}{A^I} (P_{zz}^I + r_0(P^I - P_{zz}^I)). \quad (5)$$

Here P^I and P_{zz}^I come from the fit to the signal after the area has been maximized but prior to RF modulation, A^{NMR} is the signal area and A^I is the signal area that was maximized prior to RF modulation. The values for P^I and P_{zz}^I come from Eq. 3 and 4 respectively and so the error from these terms is not large. The largest error in r_0 would be primarily from the uncertainty in Riemann sum for the remaining non-translated area. For small areas this is around 2%. There could be larger error for scenarios where the hole had not yet burned through to cleanly separate the two peaks so that a clean boundary for the Riemann sum can be established. Including the fit and area errors total error would be about 5-7% relative. This method is just a first step and is not well established but it does give a way to estimate the

polarization using the hole burning technique at various degrees of saturation. A more encompassing model and fit function will we developed in the near future. From a conservative stand point we expect to be able to achieve less than 10% relative uncertainty in the tensor polarization after hole burning.

4 Prospective Measurement

Any measurement of A_{zz} and the resulting b_1 is important to the physics community considering the single Hermes measurement and truly unexpected results for higher x . We intend to be able to measure these observables with considerably smaller errors than Hermes. We consider two cases. The first case is the case previously outline in the proposal with the advantage of minimizing the polarization errors using the fitting technology described to extract the polarization The estimated drift listed in Table 1 for each kinematic point are used along with a polarization of $\sim 20\%$. This case is shown in Fig. 1 (a) using the Kumano model for values in A_{zz} . Improving the polarization using hole burning leads to better statistics and a reduction in the drift but the over all polarization measurement uncertainty increases. The second case shows the uncertainty for optimized polarization from hole burning in which we use $\sim 30\%$ polarization. We anticipate being able to achieve much greater tensor polarization but use the value previously achieved at UVA [7]. This cases is shown in Fig. 1 (b).

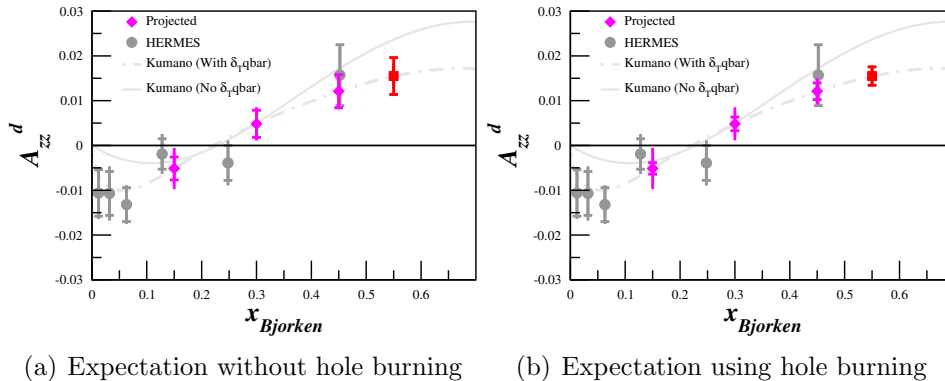


Figure 1: Demonstration of prospective error with statistical and systematic. The inside bars show the statistical uncertainty alone while the outer bar shows systematic and statistical combined.

References

- [1] Chen Yan, JLab HALL C Technical Note,
http://hallcweb.jlab.org/document/howtos/slow_raster.pdf
- [2] Russell J. Donnelly, <http://pages.uoregon.edu/rjd/vapor2.htm>

- [3] A. W. Hewat and C. Riekkel, *Acta Cryst.* (1979) A **35**, 569
- [4] C. Dulya, et al. Nucl. Instr. and Meth. in Phys. Res. A 398, 109 (1997)
- [5] W. Meyer and E. Schilling, BONN-HE-85-06, C84-09-03.1 (1985)
- [6] G.R. Court, et al. Nucl. Instr. and Meth. in Phys. Res. A 527, 253 (2004)
- [7] Results of Research Run 11/30/99-2/11/00, S. Bultmann, D. Crabb, and Y. Prok
UVA-Tech-Note (2000)